U. Walzer. Structural Classification of AB-type binary compounds. Phys. Status Solidi (b), 163:61-74, 1991.

Zentralinstitut für Physik der Erde, Institutsteil Jena[1])

Structural Classification of AB-Type Binary Compounds

By

U. WALZER

At first, a review is given on how structure maps for the prediction of the space group and structure type of AB-type binary compounds can be designed with the help of semiempirical theories. Then, two ab-initio pseudopotential theories are compared in detail. The all-electron single-particle equation and the spin-density-functional formalism form the starting point for both theories. While transferability is aimed at in both theories, the conditions imposed differ in some respects. Theory A uses the Schrödinger equation as starting point. The crossing points of a screened pseudopotential are employed as characteristic quantities. The structure energy is dominated by s-p electrons, even in the case of the compounds of two transition metals. Theory B is based on the Dirac equations and takes into account spin–orbit effects which are relevant for heavier elements. The coordinates of the minima of the bare-ion potentials serve as characteristic radii and energies. In both cases, a good separation of the structure types is achieved. For theory B, in addition, a few predictions concerning lattice constant a and the melting temperature are represented graphically.

Zunächst wird eine Übersicht gegeben, wie man mit halbempirischen Theorien Strukturkarten zur Vorhersage der Raumgruppe und des Strukturtyps binärer Verbindungen vom Typ AB entwerfen kann. Dann werden zwei ab-initio-Pseudopotentialtheorien im einzelnen verglichen. Die Einteilchengleichung für alle Elektronenschalen und der Spin-Dichte-Funktional-Formalismus sind für beide Theorien der Ausgangspunkt. Die Übertragbarkeit des Pseudopotentials auf andere chemische Umgebungen wird in beiden Theorien angestrebt, die auferlegten Bedingungen unterscheiden sich jedoch in einigen Punkten. Theorie A verwendet die Schrödinger-Gleichung als Ausgangspunkt. Als Kenngrößen werden die Nullstellen eines abgeschirmten Pseudopotentials genommen. Die Strukturenergie wird durch die s-p-Elektronen beherrscht, auch im Falle der Verbindungen zweier Übergangsmetalle. Theorie B geht von den Dirac-Gleichungen aus und setzt die Spin–Bahn-Kopplung, die für schwerere Elemente wichtig ist, in Rechnung. Als charakteristische Radien und Energien dienen die Koordinaten der Minima der Ionenrumpf-Pseudopotentiale. In beiden Fällen wird eine gute Trennung der Strukturtypen erreicht. Für Theorie B werden auch einige Voraussagen bezüglich der Gitterkonstanten a und der Schmelztemperatur graphisch gezeigt.

1. Introduction

The present paper is concerned with attempts to design structure maps, i.e. two-dimensional diagrams on the axes of which certain empirical or theoretically computed physical quantities are plotted and in which the structure types and space groups of the crystals can be topologically separated. Only those crystals may be taken which are in equilibrium under the same fixed temperature and pressure conditions. If the symbols representing the crystal structures cluster entirely or partly in separate domains, one may hope to be able to predict the structure for substances that are still unknown from the properties of the atomic constituents.

In most cases, **two** physical quantities have been employed for designing the aforementioned plots, e.g. the difference of electronegativity and the difference of a geometrical

[1]) Burgweg 11, O-6900 Jena, F.R. Germany.

quantity of the atom. However, there are also exceptions: Pettifor [1], for example, tries to define the chemical elements only by **one** quantity. He does not classify them according to the number of protons, but according to the Mendeleev number introduced by him, a new atomic number which is not in agreement with the conventional atomic number of the elements. Now he plots the symbols for the structure types of AB-type binary compounds in a diagram whose axes are formed by the new atomic number for constituent A and by the new atomic number for constituent B. The Pettifor plot indeed shows a good separation of the compounds into clusters, however, the choice of some of these new atomic numbers appears to be somewhat arbitrary.

A deviation to the other side is made by Villars [2] who constructed three-dimensional plots on the basis of **three** quantities: He employed the electronegativity difference ΔX, the size difference ΔY, and the average number of valence electrons per atom $\bar{Z}$. His structural classifications are very distinct and good, although the work with sixteen two-dimensional plots — i.e. practically three-dimensional diagrams — is not very handy. As is well known, the four types of chemical bonding, i.e. metallic, Van der Waals, ionic, and covalent bonding, mostly occur in a mixed form, i.e. the percentages with which they contribute to total bonding differ from one another. This is in conformity with the empirical finding that band effects, atomic radii, electronegativity, and hybridization are well suited for making the space groups of the crystals in the structure maps separable. Frequently, the discussion is not very clear in individual points, because different authors define the quantities, e.g. the electronegativity, in different ways. One of the earliest scales of electronegativity used to the present day is that by Allred and Rochow [3]. Pauling's scale [4] is more widely used. It is based for the major part on molecular heats of formation. In contrast to this, the electronegativity by Phillips [5] is based on fully hybridized crystalline sp^3 bonds. St. John and Bloch [6] use for nontransition elements an electronegativity which is numerically situated between the values from [4] and [5]. It is computed from the Bloch-Simons orbital radii and has, thus, been derived from quantum variables. It is the first one among these quantities which is largely independent of the molecular or crystalline environment. It might be worthwhile to mention the stages of development preceding this breakthrough: Mooser and Pearson [7, 8] at first confined themselves to the separation of nonoctet binary compounds. They used as coordinates the magnitude of the difference of Pauling's electronegativity and the average principal quantum number. They also were fairly successful in the graphical separation of compounds consisting of a transition-metal atom and a simple-metal atom with N valence electrons, however, with the restriction $3 \leqq N \leqq 6$. The separation according to crystal structures can be seen only in some parts of the graphs.

A similarly possible good separation of the crystal structures was obtained by Shaw [9] for nonoctet compounds. As dual coordinates, he also used, on the one hand, the electronegativity difference, on the other hand, however, the quantity

$$\tfrac{1}{2}(Z_A + Z_B)/[\tfrac{1}{2}(n_A + n_B)]^3 ,$$

Z_A is the atomic number, n_A the principal quantum number of the outer orbital of atom A.

A method that is only applicable to fully bonded cubic crystals was developed by Van Vechten [10] and Phillips [11]. From the bond lengths and dielectric constants of the compounds, they computed the average covalent energy gap and the average ionic energy gap. These two quantities served as variables in their structure maps for octet compounds. Miedema's [12] parameters $P_1 = |\Phi_A^* - \Phi_B^*|$ and $P_2 = |n_A^{*1/3} - n_B^{*1/3}|$ were successful in the

prediction of the heats of formation of compounds and in the determination of composition–temperature phase diagrams [13]. Φ_A^* is the effective elemental work function, n_A^* the electron density at the boundary of the Wigner-Seitz atomic cell of atom A.

However, these variables can be used only with moderate success for the separation of the crystal structures.

2. A Comparison

In the following, we will compare two pseudopotential approaches, which are both based on first principles and do not contain any fitting of parameters to experimental data. The first approach, theory A, is the theory by Zunger [14], the second one, theory B, is based on ideas of Hamann et al. [15]. The theoretical and numerical elaboration of the latter theory can be found in [16 to 19]. In both theories, the pseudopotentials have been derived from full-core atom calculations. However, there are certain differences which are to be made evident here by a comparison. In both approaches, an all-electron (ae) single-particle equation and the spin-density-functional formalism [20, 21] are used. There are differences, however, both in the fundamental equation and in the substitution of the potential by a pseudopotential. The potential in the Schrödinger-type equation is separated in both theories into an electron-nuclear attraction potential V_{ext} and an interelectron potential V_{scr}. V_{scr} contains, both Coulomb and exchange and correlation screening. In theory A, we have for the effective potential

$$V_{eff}^{ae}(\mathbf{r}) = V_{scr}^{ae}(\mathbf{r}) + V_{ext}(\mathbf{r}) . \tag{1}$$

The all-electron equation is

$$\{-(\tfrac{1}{2})\nabla^2 + V_{scr}^{ae}[\varrho_c(\mathbf{r}) + \varrho_v(\mathbf{r})] + V_{ext}(\mathbf{r})\}\,\psi_j(\mathbf{r}) = \varepsilon_j\psi_j(\mathbf{r}) ; \tag{2}$$

ϱ_c is the core charge density, ϱ_v the valence charge density. The eigenstates $[\psi_j(\mathbf{r})]$ must be orthogonal. For the charge density ϱ,

$$\varrho(\mathbf{r}) = \sum_j |\psi_j(\mathbf{r})|^2 , \tag{3}$$

while for theory B we have

$$\varrho(\mathbf{r}) = \sum_j [|G_j(\mathbf{r})|^2 + |F_j(\mathbf{r})|^2] , \tag{4}$$

because here the Schrödinger equation has been substituted by the Dirac equation in its radial form. This is an expedient approach for allowing for the influence of spin–orbit effects, which is important for the computation of the pseudopotential of heavier elements,

$$\frac{dF_j(r)}{dr} - \frac{\varkappa}{r} F_j(r) + [\varepsilon_i - V(r)]\,\alpha G_j(r) = 0 , \tag{5}$$

$$\frac{dG_j(r)}{dr} + \frac{\varkappa}{r} G_j(r) - [2/\alpha^2 + \varepsilon_j - V(r)]\,\alpha F_j(r) = 0 , \tag{6}$$

where $\varkappa$ is the relativistic quantum number and l the angular momentum quantum number, with

$$\varkappa = l \quad \text{for} \quad j = l - \tfrac{1}{2},$$
$$\varkappa = -(l+1) \quad \text{for} \quad j = l + \tfrac{1}{2},$$

and

$$c = \alpha^{-1} = 137.037 \quad \text{and} \quad \hbar = m = e = 1.$$

For the splitting of the potential in theory B, we have

$$V(r) = \int \frac{\varrho(r')}{|r - r'|}\,dr' + \frac{\delta E_{xc}[\varrho]}{\delta \varrho(r)} + V_{ext}(r). \tag{7}$$

It is, in principle, the same as in theory A. The special dependence of the exchange-correlation energy E_{xc} on ϱ of theory B is given in [19]. In theory A, the valence screening V_{scr}^{ps} has the same functional form as the all-electron screening V_{scr}^{ae}, but is a functional of the valence pseudo-charge density n. Consequently, the pseudopotential single-particle equation of theory A is

$$\{-(\tfrac{1}{2})\nabla^2 + V_{scr}^{ps}[n(\mathfrak{r})] + V_{ps}(\mathfrak{r}, \mathfrak{r}')\}\,\chi_j(\mathfrak{r}) = \tilde{\varepsilon}_j \chi_j(\mathfrak{r}) \tag{8}$$

with

$$n(\mathfrak{r}) = \sum_j |\chi_j(\mathfrak{r})|^2. \tag{9}$$

In theory A, the external potential V_{ext} is **directly** replaced by the pseudopotential V_{ps}, and the transferability is achieved by physical constraints on the pseudo-wave functions $\chi_j(\mathfrak{r})$. The atomic pseudopotential thus obtained is almost independent of energy and state. Two conditions imposed on the pseudopotentials in the two theories are in agreement:

Firstly, real and pseudo-valence eigenfunctions are in conformity in a prototype atomic configuration, i.e. $\tilde{\varepsilon}_{nl} = \varepsilon_{nl}$. Secondly, real and pseudo-atomic wave functions are in conformity for radii r which are greater than a chosen core radius r_c.

For theory A **alone**, a special choice of unitary rotation coefficients $\{C_{n,n'}^{(l)}\}$ is required:

$$\chi_{nl}(r) = \sum_{n'} C_{n,n'}^{(l)} \varphi_{n'l}^{c,v}(r). \tag{10}$$

The following considerations serve for the explanation of this formula: the pseudo-wave functions $\{\chi_{nl}(r)\}$ are the lowest solutions to

$$\{-(\tfrac{1}{2})\nabla^2 + v_{ps}^{(l)}(r)\,\hat{P}_l + l(l+1)/2r^2 + v_{ee}[n(r)] + v_x[n(r)] + v_{cr}[n(r)]\}\,\chi_{nl}(r) = \tilde{\varepsilon}_{nl}\chi_{nl}(r). \tag{11}$$

The variable v_{ee} denotes the atomic screening potential of the electrostatic interaction between the electrons, v_x the exchange term, and v_{cr} the correlation term. $\hat{P}_l$ is the projection operator. It is required for the computation of the total pseudopotential $V_{ps}(\mathfrak{r}, \mathfrak{r}')$ for crystals and other more complicated systems through the superposition of atomic pseudopotentials,

$$V_{ps}(\mathfrak{r}, \mathfrak{r}') = \sum_{\mathfrak{R}_n} v_{ps}^{(l)}(\mathfrak{r} - \mathfrak{R}_n)\,\hat{P}_l.$$

The atoms are situated at the lattice points $\mathfrak{R}_n$. The real wave functions $\{\psi_{nl}(r)\}$ originate from the all-electron equation

$$\{-(\tfrac{1}{2})\nabla^2 - (Z_c + Z_v)/r + l(l+1)/2r^2 + v_{ee}[\varrho_c(r) + \varrho_v(r)] + v_x[\varrho_c(r) + \varrho_v(r)] + v_{cr}[\varrho_c(r) + \varrho_v(r)]\}\,\psi_{nl}(r) = \varepsilon_{nl}\psi_{nl}(r)\,. \tag{12}$$

Index c stands for core, v for valence, Z is the number of electrons.

In theory B, on the other hand, the additional conditions for establishing the transferability are as follows: thirdly, the integrals from 0 to r of the real and charge densities are in conformity for each valence state for $r > r_c$.

Fourthly, for $r > r_c$ the logarithmic derivatives of the real and pseudo-wave function are in conformity. The same applies also to their first energy derivatives.

In theory B, the definition of the pseudopotential is much more complicated. From (5) and (6), there follows at first approximately a Schrödinger-type equation from which the major wave function component $G_j(r)$ can be computed. Therefrom, a first-step pseudopotential $\hat{V}_{1j}^{(v)}$ is derived, with the singularity near $r \approx 0$ being cut off in the **screened** full-core potential $V^{(v)}$. The computation is performed independently for each angular-momentum quantum state, with

$$\hat{V}_{1j}^{(v)} = V^{(v)}[1 - \exp[-(r/r_{cj})^{3.5}]] + c_j^{(v)} \exp[-(r/r_{cj})^{3.5}]\,.$$

The cut-off radius r_{cj} is not an adjustable parameter. The constant $c_j^{(v)}$ is determined so that $\tilde{\varepsilon}_{nl} = \varepsilon_{nl}$, as has already been demanded. After a few further steps (see [17 to 19]), the screened pseudopotential $\hat{V}_{2j}^{(v)}(r)$ is unscreened by the valence electrons,

$$\hat{V}_{l\pm 1/2}^{\text{ion}} = \hat{V}_{2j}^{(v)}(r) - \int \frac{\varrho^{(v)}(r')}{|r - r'|}\,\mathrm{d}r' - \frac{\delta E_{xc}[\varrho^{(v)}]}{\delta \varrho^{(v)}(r)}\,. \tag{13}$$

This valence unscreening signifies a linearization of the exchange-correlation energy as a function of $\varrho^{(v)}$.

3. Classification

The bare-ion pseudopotentials of theory B which can be numerically computed from (13) will now be graphically represented in a few examples. $\hat{V}_{l-1/2}^{\text{ion}}$ and $\hat{V}_{l+1/2}^{\text{ion}}$ differ above all for heavier elements. This is already the case for iron which most probably has a dominating share in the cores of the terrestrial planets. The strength of the spin–orbit effects results from

as the crossing points of the pseudopotentials of theory A. We will define our characteristic radii and energies (potentials) essentially as the minima of the potentials after theory B, which are reached first coming from the infinite radius r. In this way, these new characteristic quantities are most easily comparable to the electronegativity, i.e. they are approximately linearly correlated with it. Contrary to [14], we will not classify the experimental comparative material, subdividing it into octet, suboctet, and superoctet crystals according to the classical valence-electron concentration. This would of course enable a better separation into separate domains in the plots, however, the assignment of an AB-type binary compound to one of the three categories is sometimes somewhat arbitrary. We have dispensed with this additional distinction in order to remain objective and to have our diagrams plotted without any corrections by the plotter of the computer. For all chemical elements from hydrogen up to plutonium, we now have computed the bare-ion pseudopotentials as a function of the distance r from the atom centre for all relevant angular momentum quantum numbers l and for both spin states. For the purpose of classification, new characteristic quantities were determined from these curves, as far as this was possible,

$$\begin{aligned} &r_{m0}, v_{m0}, e_{m0}; \quad r_{m1}, v_{m1}, e_{m1}; \quad r_{p1}, v_{p1}, e_{p1}; \\ &r_{m2}, v_{m2}, e_{m2}; \quad r_{p2}, v_{p2}, e_{p2}; \quad r_{m3}, v_{m3}, e_{m3}; \end{aligned} \tag{15}$$

r is the radius, v the pseudopotential of the characteristic point. Both are expressed in atomic units. The pertaining genuineness is 1, if the point on the curve represents the first potential minimum that is reached coming from the infinite r, and if this minimum is not situated at $r = 0$. If the minimum is at $r = 0$, then $e = 0$. In this case, the pair of numbers r, v designates the point of the curve where, simultaneously, $\frac{d^2v}{dr^2} > 0$ and the curvature k, coming from infinitely large r, assumes a maximum, with

$$k = \frac{d^2v}{dr^2}\left[1 + \left(\frac{dv}{dr}\right)^2\right]^{-3/2}. \tag{16}$$

The indices m in (15) relate to the following equation

$$\hat{V}^{\text{ion}}_{l-1/2}(r) = \hat{V}^{\text{ion}}_{l}(r) - ((l+1)/2)\,\hat{V}^{\text{so}}_{l}(r)\,, \tag{17}$$

the indices p, on the other hand, to

$$\hat{V}^{\text{ion}}_{l+1/2}(r) = \hat{V}^{\text{ion}}_{l}(r) + \left(\frac{l}{2}\right)\hat{V}^{\text{so}}_{l}(r)\,. \tag{18}$$

The second index of (15) stands for the angular momentum quantum number. Fig. 1 shows the pseudopotentials of a few elements. With phosphorus, the splitting of the curves (17) and (18) is only weakly indicated for $l = 1$ and appears only in the form of a line thickening. With germanium, but in particular with tantalum, the relativistic bifurcation can be clearly seen. The characteristic points (15), marked by short strokes on the curves, were determined by means of the computer. The theoretical quantities represented in Fig. 2 to 10 originate from theory B, the experimental values from the encyclopaedia by Villars and Calvert

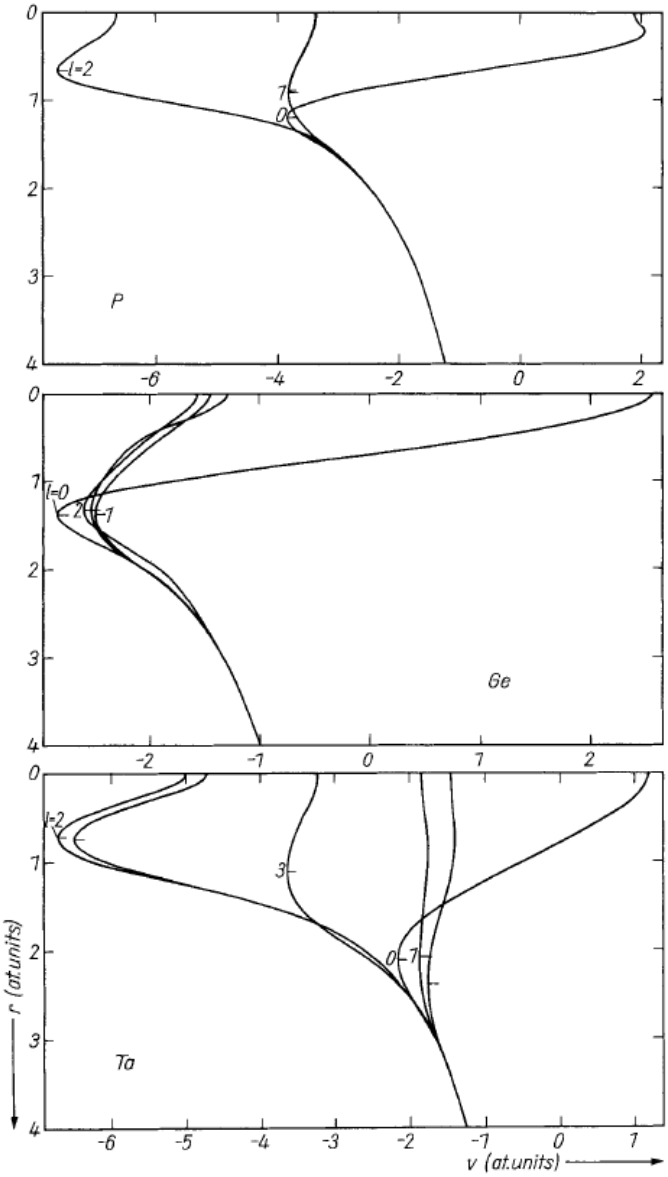

Fig. 1. The pseudopotentials of phosphorus, germanium, and tantalum, computed by means of (17) and (18)

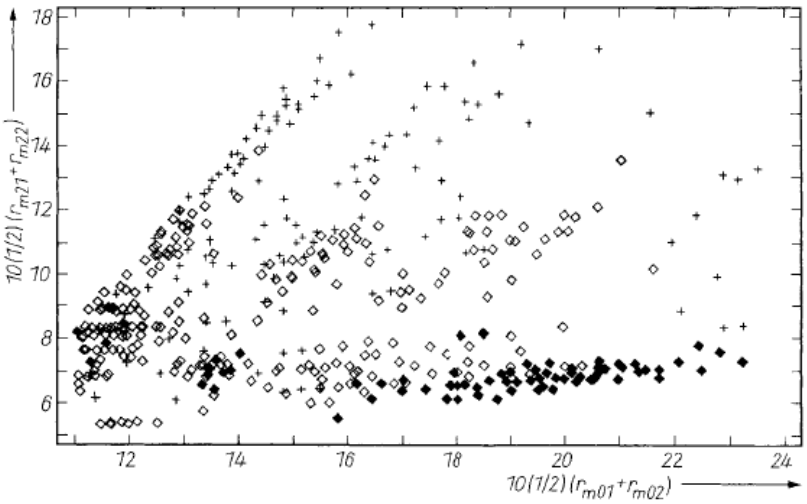

Fig. 2. Radius–radius diagram (in at. units). On the abscissa, 10 (1/2) ($r_{m01} + r_{m02}$) is plotted, and on the ordinate, 10 (1/2) ($r_{m21} + r_{m22}$). Solid diamonds represent compounds and alloys of two transition metals (TT), crosses two simple metals (SS). Open diamonds represent the compounds and alloys of a transition metal and of a simple metal (ST)

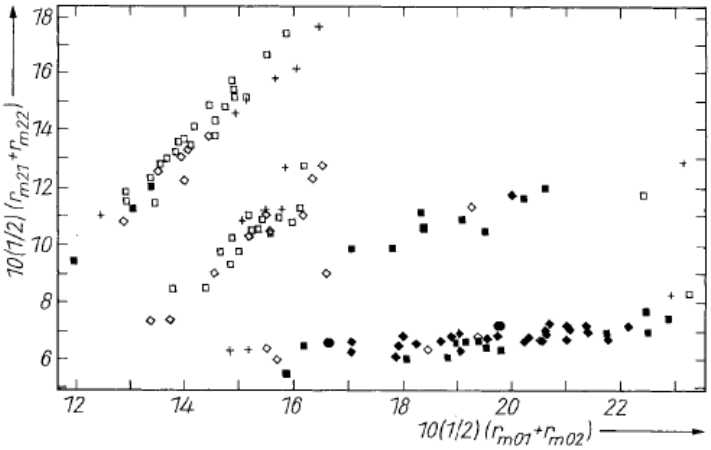

Fig. 3. Radius–radius diagram. On the coordinates, the same quantities are plotted as in Fig. 2; however, not all compounds and alloys have been permitted here, but only those consisting of elements of the fourth, fifth, and sixths periods of the Periodic Table with the exception of the rare-earth elements. The symbols represent intervals of the melting temperature T_m in K.

Solid diamonds	$T_m \geqq 2028$,
solid squares	$2028 > T_m \geqq 1487$,
open diamonds	$1487 > T_m \geqq 946$,
open squares	$946 > T_m \geqq 405$,
crosses	$405 > T_m$

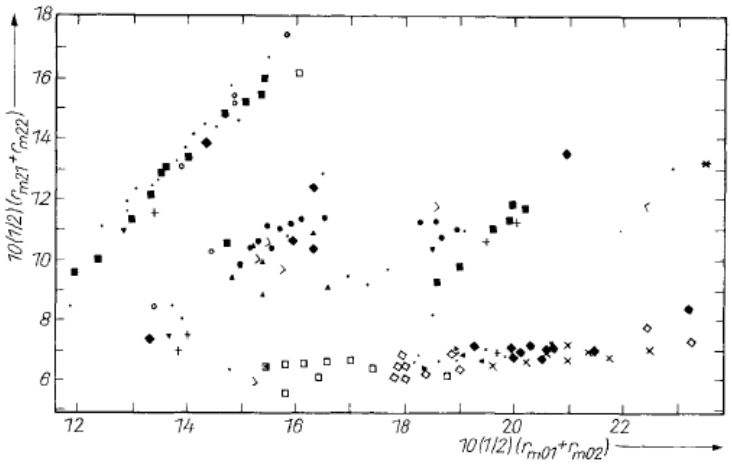

Fig. 4. Radius–radius diagram. On the coordinates, the same quantities are plotted as in Fig. 2. As in Fig. 3, the diagram is limited to elements of the fourth, fifth, and sixth periods without lanthanides. The symbols denote the space group and structure type of the crystal lattice. For more details, see Table 1

[22]. Unless specified otherwise, the quantities are represented in at. units. In Fig. 2 to 4, the same simple combination of the characteristic radii has each time been plotted on the axes, on the abscissa the mean value of the radii for d-electrons and on the ordinate the mean value of the radii for s-electrons. The last index of the quantities used for explaining the figures denotes the type of atom. The varying number of measuring points in Fig. 3 and 4 is simply due to the fact whether the melting temperature and the lattice type are known. Here, as in the other figures, no points were excluded. Fig. 2 and Fig. 3 show that the types TT, ST, and SS are by no means randomly distributed. If, for example, the theoretical computation yields a mean to high value for the mean of the radii for s-electrons and a low value for that of d-electrons, we mostly have to do with TT with a higher melting temperature. Above all in Fig. 3 and 4, the experimental points are clearly arranged in clusters. Good predictions as to the lattice constants can be made from a radius–potential diagram for s-electrons (see Fig. 5). Fig. 6 shows that, on lines with an identical lattice structure, also the lattice structure can be predicted to a certain extent. Fig. 7 demonstrates that the space group and structure type can be predicted for many areas of the theoretically computed diagram. A similar representation for all lattices is given in Fig. 8. Certain lines are dominated here by certain structure types, so that predictions are still possible in this mixture of types without a separation into TT, ST, and SS. The properties can be predicted with greater certainty by the combination of several diagrams. Many of these plots have not been printed here for reasons of space. From the Bloch-Simons [6] orbital shell radii $r_s^{(\alpha)}$ and $r_p^{(\alpha)}$, two quantities, r_π and r_σ, have formerly been defined

$$r_\pi = r_\pi^{(1)} + r_\pi^{(2)} \quad \text{and} \quad r_\sigma = r_\sigma^{(1)} - r_\sigma^{(2)},$$

the numbers relating to two types of atoms, and

$$r_\pi^{(\alpha)} = r_p^{(\alpha)} - r_s^{(\alpha)} \quad \text{and} \quad r_\sigma^{(\alpha)} = r_s^{(\alpha)} + r_p^{(\alpha)}.$$

Table 1
The assignment of symbols for the plots in which the symbols express the space group of the crystal lattice

space group	structure type	symbol	description of symbol
$Fm\bar{3}m$	ClNa	■	solid square
$Fm\bar{3}m$	Cu	□	open square
$F\bar{4}3m$	SZn	○	open circle
$Fd\bar{3}m$	NaTl	^	right angle, tip pointing upward
$Pm\bar{3}m$	ClCs	◆	solid diamond
$P6_3/mmc$	AsNi	●	solid circle
$P6_3/mmc$	Mg	◇	open diamond
$P6_3mc$	SZn	v	right angle, tip pointing downward
Pnma	BFe	▼	solid triangle, tip pointing downward
Pnma	MnP	▲	solid triangle, tip pointing upward
P4/mmm	AuCu	◀	solid triangle, tip pointing to the left
P4/nmm	CuTi	▶	solid triangle, tip pointing to the right
$P\bar{4}3n$	GeK	<	right angle, tip pointing to the left
$P2_13$	FeSi	>	right angle, tip pointing to the right
Cmcm	BCr	+	upright cross
$Im\bar{3}m$	W	×	oblique cross
$I4_1/acd$	NaPb	*	oblique cross with additional horizontal beam

According to [23], $r_\pi^{(\alpha)}$ corresponds to the p^2-sp hybrids, the quantity $r_\sigma^{(\alpha)}$, on the other hand, to the s-p σ hybrids. Analogously, based on **our** characteristic radii, we define the following quantities, the first one being a kind of size mismatch,

$$R_\sigma^{(w)} = |(r_{11} + r_{m01}) - (r_{12} + r_{m02})|\,, \tag{19}$$

with

$$r_{11} = (r_{m11} + r_{p11})/2 \quad \text{and} \quad r_{12} = (r_{m12} + r_{p12})/2\,. \tag{20}$$

A measure for the sum of the orbital nonlocality is obtained from

$$R_\pi^{(w)} = |r_{11} - r_{m01}| + |r_{12} - r_{m02}|\,. \tag{21}$$

In [19], it has been shown that, with the help of these dual coordinates, particularly good separations according to the crystal structure are possible. Fig. 9 serves here as a fairly good

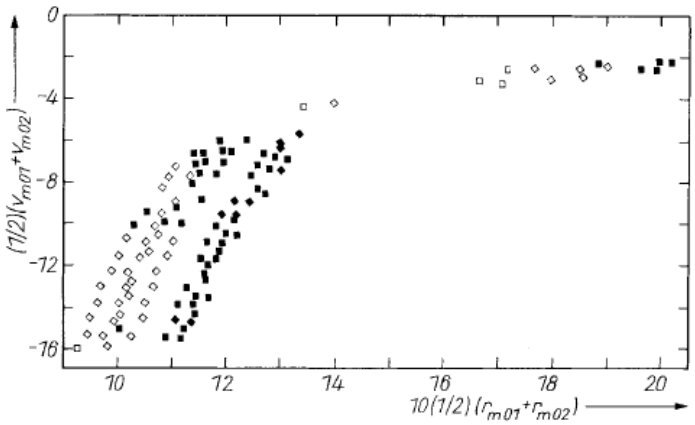

Fig. 5. Radius–potential diagram with 10 (1/2) ($r_{m01} + r_{m02}$) on the abscissa and (1/2) ($v_{m01} + v_{m02}$) on the ordinate. Only compounds and alloys of one simple and one transition metal (ST) each with NaCl lattices as symbols were plotted. These symbols represent the following intervals of the lattice constants a (in 10^{-10} m).

Solid diamonds	$a \geqq 6.3665$,
solid squares	$6.3665 > a \geqq 5.8517$,
open diamonds	$5.8517 > a \geqq 5.3369$,
open squares	$5.3369 > a \geqq 4.8221$,

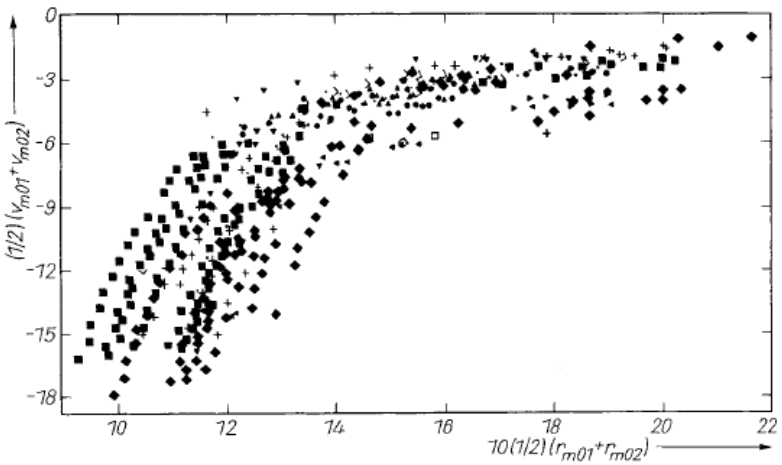

Fig. 6. Radius–potential diagram. The coordinates represent the same quantities as in Fig. 5. Also here, only ST has been plotted in symbols. The symbols denote the space group and structure type of the crystal lattice. For further explanations, see Table 1

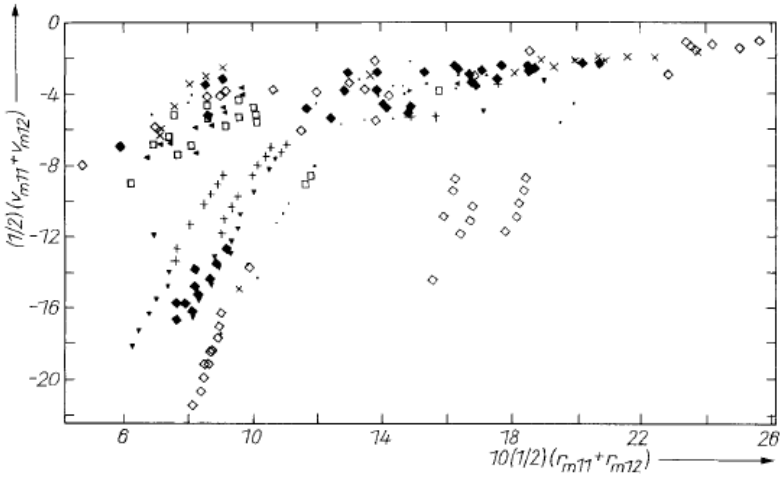

Fig. 7. Radius–potential diagram with 10 (1/2) ($r_{m11} + r_{m12}$) on the abscissa, but with (1/2) ($v_{m11} + v_{m12}$) on the ordinate. The symbols represent the lattice type of TT according to Table 1

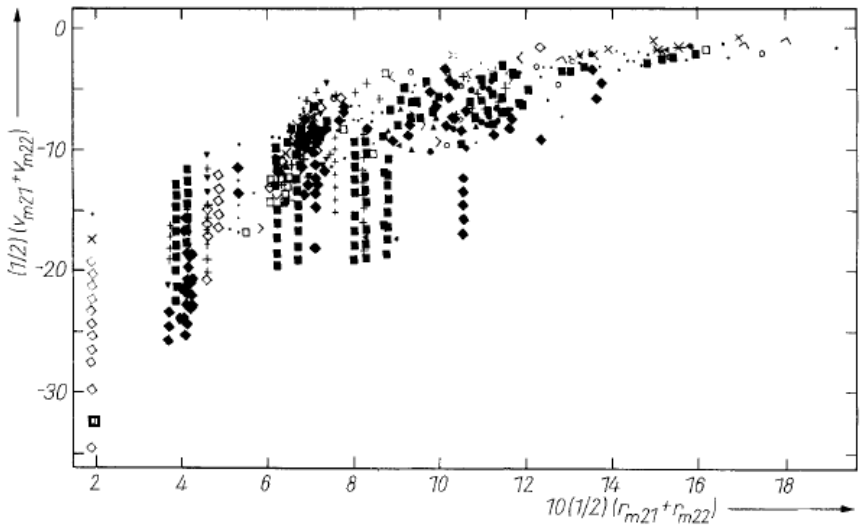

Fig. 8. Radius–potential diagram for d-electrons. On the abscissa, 10 (1/2) ($r_{m21} + r_{m22}$) is plotted, and on the ordinate (1/2) ($v_{m21} + v_{m22}$). In the representation, all lattices have been used. The symbols denote the space group and structure type of the crystal lattice. See Table 1

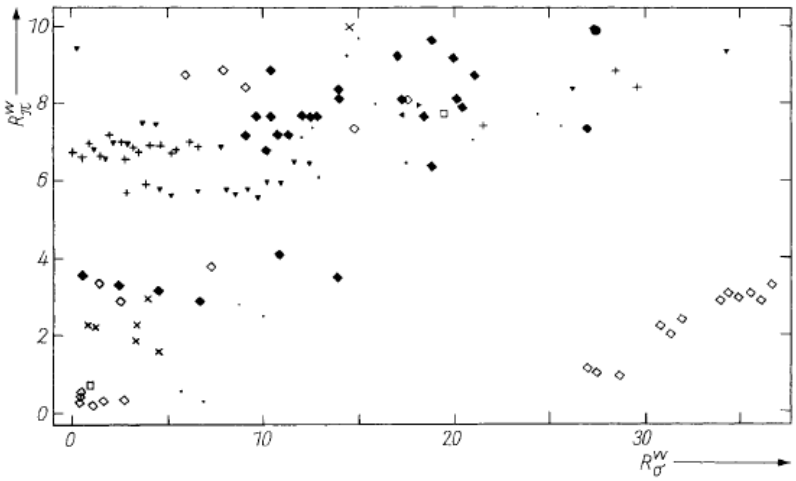

Fig. 9. On the abscissa, $R_\sigma^{(w)}$ is plotted, on the ordinate, $R_\pi^{(w)}$. The symbols represent the crystal lattices. For more details, see Table 1

example. For Fig. 10, a simple function F was used which results from $F = \frac{1}{2}(F_1 + F_2)$ and

$$F_\alpha = 10\,\frac{s_p - 1}{18 - 1}\,(r_{m0\alpha} - 1)\,v_{m0\alpha}\,, \tag{22}$$

s_p is the column in the Periodic Table. α is 1 or 2, depending on the type of atom. For compounds and alloys of two transition metals (TT), we observe an increase in the melting temperarature with F. For higher temperatures, the areas covered by TT, ST, and SS are clearly separated.

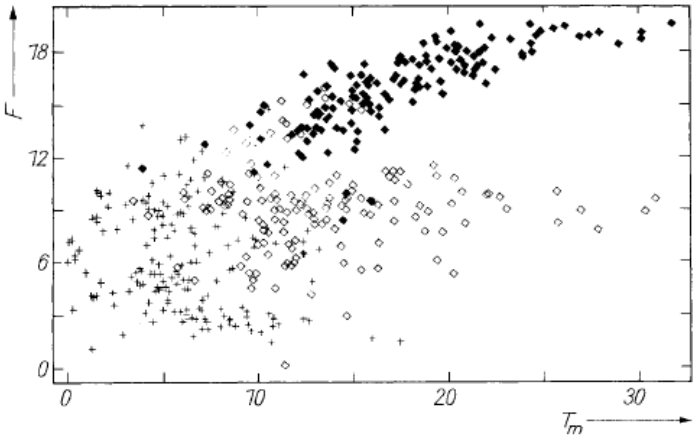

Fig. 10. T_m–F diagram. On the abscissa the melting temperature T_m is plotted in 100 °C, on the ordinate the theoretically computed function F according to (22) in at. units. Solid diamonds represent TT, open diamonds ST, crosses SS

4. Conclusions

After an introduction into the preparation of structure maps with semi-empirical theories, two pseudopotential theories, A and B, are compared, which are based on first principles and for which an optimum transferability to various systems was attempted. For theory B, the applicability is shown in figures. Characteristic quantities were determined for each pseudopotential curve. With the help of plots, space group and structure type of the crystals, the lattice constants, the melting temperature, and other physical quantities can be predicted. In theory B, also the pseudopotential curves for the d-electrons play a role, while in theory A, the influence of the d-electrons is only indirect, even for intermetallic compounds of two transition metals.

References

[1] D. PETTIFOR, New Scientist 29 May, 48 (1986).
[2] P. VILLARS, J. less-common Metals **92**, 215 (1983).
[3] A. L. ALLRED and E. G. ROCHOW, J. inorg. nuclear Chem. **5**, 264 (1958).
[4] L. PAULING, The Nature of the Chemical Bond, 3rd ed., Cornell University Press, Ithaka (N.Y.) 1967.
[5] J. C. PHILLIPS, Bonds and Bands in Semiconductors, Academic Press, New York 1973.
[6] J. ST. JOHN and A. N. BLOCH, Phys. Rev. Letters **33**, 1095 (1974).
[7] E. MOOSER and W. B. PEARSON, Acta cryst. **12**, 1015 (1959).
[8] W. B. PEARSON, Development in the Structural Chemistry of Alloy Phases, Ed. B. C. GIESSEN, Plenum Press, New York 1969.
[9] R. W. SHAW, Phys. Rev. **174**, 769 (1968).
[10] J. A. VAN VECHTEN, Phys. Rev. **182**, 891 (1969).
[11] J. C. PHILLIPS, Rev. mod. Phys. **42**, 317 (1970).
[12] A. R. MIEDEMA, J. less-common Metals **46**, 67 (1976).
[13] F. R. DE BOER, R. BOOM, W. C. M. MATTENS, A. R. MIEDEMA, and A. K. NIESSEN, Cohesion in Metals–Transition Metal Alloys, North-Holland, Amsterdam 1988.
[14] A. ZUNGER, A Pseudopotential Viewpoint of the Electronic and Structural Properties of Crystals, in: Structure and Bonding in Crystals, Vol. I, Academic Press, 1981.
[15] D. R. HAMANN, M. SCHLÜTER, and C. CHIANG, Phys. Rev. Letters **43**, 1494 (1979).
[16] G. B. BACHELET, H. S. GREENSIDE, G. A. BARAFF, and M. SCHLÜTER, Phys. Rev. B **24**, 4745 (1981).
[17] G. B. BACHELET, D. R. HAMANN, and M. SCHLÜTER, Phys. Rev. B **26**, 4199 (1982).
[18] H. S. GREENSIDE and M. SCHLÜTER, Phys. Rev. B **28**, 535 (1983).
[19] U. WALZER, phys. stat. sol. (b), **162**, 75 (1990).
[20] P. C. HOHENBERG and W. KOHN, Phys. Rev. **136**, 864 (1964).
[21] W. KOHN and L. J. SHAM, Phys. Rev. **140**, 1133 (1965).
[22] P. VILLARS and L. D. CALVERT, Pearson's Handbook of Crystallographic Data for Intermetallic Phases, Vol 1 to 3, American Society for Metals, Metals Park (Ohio) 1985.
[23] J. C. PHILLIPS, Solid State Commun. **22**, 549 (1977).

(Received August 1, 1990)